RK-33, a small molecule inhibitor of host RNA helicase DDX3, suppresses multiple variants of SARS-CoV-2

Farhad Vesuna[1†], Ivan Akhrymuk[2†], Amy Smith[2],
Paul T. Winnard Jr[1], Shih-Chao Lin[3], Lauren Panny[2],
Robert Scharpf[4], Kylene Kehn-Hall[2,5]* and Venu Raman[1,6,7]*

[1]Division of Cancer Imaging Research, Department of Radiology, Johns Hopkins University School of Medicine, Baltimore, MD, United States, [2]Department of Biomedical Science and Pathobiology, Virginia-Maryland College of Veterinary Medicine, Virginia Polytechnic Institute and State University, Blacksburg, VA, United States, [3]Bachelor Degree Program in Marine Biotechnology, College of Life Sciences, National Taiwan Ocean University, Keelung, Taiwan, [4]Division of Biostatistics and Bioinformatics, Department of Oncology, Johns Hopkins University School of Medicine, Baltimore, MD, United States, [5]Center for Zoonotic and Arthropod-borne Pathogens, Virginia Polytechnic Institute and State University, Blacksburg, VA, United States, [6]Departments of Oncology, Pharmacology and Molecular Sciences, Johns Hopkins University School of Medicine, Baltimore, MD, United States, [7]Department of Pathology, University Medical Center Utrecht, Utrecht, The Netherlands

SARS-CoV-2, the virus behind the deadly COVID-19 pandemic, continues to spread globally even as vaccine strategies are proving effective in preventing hospitalizations and deaths. However, evolving variants of the virus appear to be more transmissive and vaccine efficacy toward them is waning. As a result, SARS-CoV-2 will continue to have a deadly impact on public health into the foreseeable future. One strategy to bypass the continuing problem of newer variants is to target host proteins required for viral replication. We have used this host-targeted antiviral (HTA) strategy that targets DDX3X (DDX3), a host DEAD-box RNA helicase that is usurped by SARS-CoV-2 for virus production. We demonstrated that targeting DDX3 with RK-33, a small molecule inhibitor, reduced the viral load in four isolates of SARS-CoV-2 (Lineage A, and Lineage B Alpha, Beta, and Delta variants) by one to three log orders in Calu-3 cells. Furthermore, proteomics and RNA-seq analyses indicated that most SARS-CoV-2 genes were downregulated by RK-33 treatment. Also, we show that the use of RK-33 decreases TMPRSS2 expression, which may be due to DDX3s ability to unwind G-quadraplex structures present in the TMPRSS2 promoter. The data presented support the use of RK-33 as an HTA strategy to control SARS-CoV-2 infection, irrespective of its mutational status, in humans.

KEYWORDS

SARS-CoV-2, host-targeted antiviral, RNA helicase, DDX3 inhibitor, RK-33, viral isolates, TMPRSS2

Introduction

The causative agent of the worldwide COVID-19 pandemic is the Severe Acute Respiratory Syndrome Coronavirus 2 (SARS-CoV-2). Vaccines are generally considered as the first line of defense against such a large-scale viral spread. Basically, vaccines prime the host's immune system, which then coordinates a direct attack against specific

virions. Indeed, rapid deployment of several safe COVID-19 vaccines has proven very effective in attenuating infections and limiting deaths. Nevertheless, as with all viruses, SARS-CoV-2 has been evolving/mutating and variants that are more transmissible have emerged (Joshi et al., 2021; Singh et al., 2021). Moreover, it is possible that the continuous evolution of SARS-CoV-2 will result in a vaccine resistant variant(s) (Singh et al., 2021) even as the efficacy of vaccines is waning (Chemaitelly et al., 2021; Fowlkes et al., 2021; Goldberg et al., 2021). Accordingly, SARS-CoV-2 will continue to have a major impact on the future of public health if development of alternative therapeutic strategies are not pursued.

Direct-acting antiviral agents (DAAs) and host-targeted antivirals (HTAs) have been developed into effective alternatives to vaccine resistance or for use in combination with vaccinations (Kumar et al., 2020). Here, we have used a HTA directed against the human host DEAD (Asp-Glu-Ala-Asp)-box RNA helicase, DDX3X (DDX3) and demonstrated a potential of providing an anti-SARS-CoV-2 therapy. We developed a small molecule inhibitor of DDX3, RK-33, that is designed to be a competitive inhibitor of the DDX3 ATP-binding site and has been demonstrated to abrogate its RNA helicase function (Bol et al., 2015; Xie et al., 2016; Heerma van Voss et al., 2018) which is required for the translation of complex structured 5′capped mRNAs. In addition, using highly accurate physical and biochemical methodologies such as, analytical ultracentrifugation, binding kinetics, and isothermal titration calorimetry, it has been demonstrated that RK-33 binds DDX3 within the Walker I motif that contributes to ATP-binding (Yang et al., 2020). Our rationale was based on evolutionary studies of SARS-CoV-2, which have revealed that it is closely related to SARS-CoV with a similar sized genome that has nearly identical organization and hence, replication (van den Born et al., 2005; Stammler et al., 2011; Yang and Leibowitz, 2015; Coronaviridae Study Group of the International Committee on Taxonomy of Viruses, 2020; Petrosillo et al., 2020; Yoshimoto, 2020). SARS-CoV-2 replication initially proceeds through a 5′cap-dependent translation using the host's translation complexes (Cencic et al., 2011). Consequently, SARS-CoV-2 also has a 5′capped mRNA genome that requires cap-dependent translation (Gordon et al., 2020b). Given the strong evidence that DDX3 participates in 5′capped translation where it forms functional complexes with several eukaryotic translation initiation co-factors including eIF4E, eIF4F, eIF4G and eIF3 (Lee et al., 2008; Geissler et al., 2012; Shih et al., 2012; Soto-Rifo and Ohlmann, 2013) and is a required functioning unit in promoting translational as a part of the 80S translation initiation complex (Geissler et al., 2012), it follows that DDX3 would be utilized in the translation of the SARS-CoV-2 genome. Consistent with this line of reasoning, recent proteomics analyses found DDX3 colocalized with SARS-CoV-2 viral particles and the latter required DDX3 for virion production (Ciccosanti et al., 2021), DDX3 interacted with SARS-CoV-2 RNA (Kamel et al., 2021), and that DDX3 was part of the SARS-CoV-2 interactome (Schmidt et al., 2021).

Similarly, DDX3 also participates in the resolution of both RNA and DNA G-quadraplex structures and such structures have been predicted to form in the SARS-CoV-2 genome (Herdy et al., 2018; Ji et al., 2021; Russon et al., 2021), in the promoter region of the host TMPRSS2 gene (Shen et al., 2020), as well as in the 5′UTR of the TMPRSS2 transcript. TMPRSS2 expression is also required for SARS-CoV-2 entry into cells (Baughn et al., 2020; Hoffmann et al., 2020; Qiao et al., 2020). In addition, three related lines of evidence indicate that DDX3 can be considered as a prime host protein to target (Winnard et al., 2021): (a) several viruses (18 species from 12 genera and 11 families) have been demonstrated as requiring DDX3 for efficient virion production; (b) investigators have actively pursued the targeting of DDX3 with small molecule inhibitors as an antiviral strategy (Schroder, 2011; Valiente-Echeverria et al., 2015; Brai et al., 2016, 2019a,b, 2020a,b; Kukhanova et al., 2020; Quaranta et al., 2020; Yang et al., 2020); and (c) RK-33 has effectively been used to target DDX3 and abrogate virion production in Dengue, West Nile, Zika, Respiratory Syncytial, and human Parainfluenza Type-3 viral infections (Yang et al., 2020).

Our results indicate that regardless of the SARS-CoV-2 isolate (Lineage A, and Lineage B Alpha, Beta, and Delta variants), RK-33 treatment of Calu-3 cells infected with these isolates display significantly reduced viral load by one to three log orders. Consistent with this finding, proteomics and RNA-seq analyses of the infected/RK-33 treated cells demonstrated the downregulation of most of the SARS-CoV-2 proteins and genes and host TMPRSS2 expression was decreased as well. Collectively, the data obtained indicates that the use of RK-33 to abrogate host DDX3 functions is a viable option for the treatment of SARS-CoV-2 infection as well as subsequent variants that may arise.

Materials and methods

Virus inhibitor

RK-33 was dissolved in 100% DMSO to make a 10mM stock. For a cell-based assay the stock was diluted in complete cell media to required concentrations.

Cell culture and viruses

Calu-3 (ATCC HTB-55) cells were cultured at 37°C and 5% CO_2 in EMEM supplemented with 10% FBS, 1% L-glutamine, and 1% penicillin–streptomycin. Vero (ATCC CCL-81) and RD cells (human rhabdomyosarcoma cell; ATCC: CCL-136) were cultured at 37°C and 5% CO_2 in DMEM supplemented with 10% FBS, 1% L-glutamine, and 1% penicillin–streptomycin. The following SARS-CoV-2 isolates, obtained from BEI Resources,

were used in the study: Lineage A (NR-52281), Beta variant (NR-54008), Alpha variant (NR-54000), Delta variant (NR-55611).

CC$_{50}$ and EC$_{50}$

For CC$_{50}$ assays cells were maintained as described above in 96-well opaque white wall plates for 24 h prior to RK-33 drug treatment. Cells (2.8×10^4) were incubated with RK-33 in serially diluted concentrations from 50-0.39 μM for 24 h. Cell viability was estimated by CellTiter-Glo assay (Promega) in accordance with manufacturer's recommendation. For EC$_{50}$ assays Calu-3 cells were maintained as described above in 12-well plates for 24 h prior to EC$_{50}$ assays. Cells were treated with RK-33 in decreasing concentrations from 5-0.3 μM for 1 h followed by 1 h of SARS-CoV-2 Lineage A variant infection at multiplicity of infection (MOI) of 0.1. After incubation, viral infectant was removed, cells were washed once with PBS and fresh complete medium supplemented with RK-33 in equivalent concentrations was added. Virus containing cell media was collected 48 hours post infection (hpi) and virus titers were estimated by standard plaque assay as described elsewhere (Juarez et al., 2013; Mendoza et al., 2020).

Cell infection

Calu-3 cells (8×10^5) were plated in 12-well plates 24 h prior to drug treatment. Cells were then incubated with RK-33 at 5 μM concentration for 24 h followed by infection with SARS-CoV-2 variant as indicated, at MOI of 0.1. The infectant was removed after 1 h and cells were washed once with PBS and fresh complete medium supplemented with RK-33 at 5 μM concentration was added. Cells infected with SARS-CoV-2 as well as virus containing supernatants were collected 48 h post infection.

RNA-Seq

Total RNA was extracted from virus containing cell lysates using Trizol LS (Invitrogen, Carlsbad, CA) and purified using a column purification method (Qiagen, Germany) in accordance with manufacturer's recommendations that were modified to isolate both small and large RNA species. RNA concentration and preliminary quality control was estimated on a NanoDrop spectrophotometer (ThermoFisher Scientific) while RNA-Seq was performed commercially (BGI Americas, San Jose, CA) as detailed in Supplementary Methods. Four biological replicates were analyzed from each of the treatments (Uninfected cells treated with DMSO, Uninfected cells treated with RK-33, Infected cells treated with DMSO, and Infected cells treated with RK-33).

RNA-Seq data is in the process of being uploaded to the data server.

Proteomics

Proteomics was performed at the Johns Hopkins University School of Medicine Mass Spectrometry and Proteomics Core using 50 μg of each sample as detailed in Supplementary Methods. Biological replicates of four were analyzed as in RNA-Seq.

RT-qPCR and RNA isolation

Viral RNA was extracted from virus containing cell media and from cell lysates using Trizol LS (from Invitrogen, cat# 10296010) and purified by Direct-Zol RNA purification kit (from Zymo research, cat#R2052) in accordance with manufacturer's recommendations. SARS-CoV-2 RNA (RdRp and E genes) was amplified by the one-step Logix Smart-2 COVID-19 real-time PCR reagents kit from Co-Diagnostics, Inc. (Salt Lake City, UT, United States). Normalization was performed using RNaseP gene amplified from host RNA. Copy numbers were estimated based on the included quantified positive control reagent.

Mutational analysis

The genome sequence of the Lineage A variant was retrieved from GenBank accession MW811435, a direct submission of NR-52281 sequencing at ATCC. The Alpha variant genome sequence was retrieved from GenBank accession MZ376737. The Beta variant genome sequence was retrieved from GenBank accession MZ345001. The Delta variant genome sequence was reconstructed from GenBank accession MN908947 with variations as reported on the NR-55611 Certificate of Analysis. Of particular note is a deletion within ORF7a (AA 44–100) with a frameshift that results in extension of the protein sequence with a new stop codon downstream of ORF7b.

Protein sequences for 25 SARS-CoV-2 proteins were extracted from the four genome sequences. For each protein, a four-isolate multiple sequence alignment was performed in CLC Genomics Workbench with a progressive alignment algorithm using default parameters. Differences with respect to the Lineage A variant were noted. Evolutionary distances of proteins were estimated using the WAG substitution model (Whelan and Goldman, 2001).

Three-dimensional structural models of the reference A lineage spike protein homotrimer in open and closed conformations were obtained from the Zhang Lab.[1] This model was generated using the D-I-TASSER/ C-I-TASSER pipeline (Zheng et al., 2021). The protein sequence of the structural model is identical to that of the Lineage A variant used in this study. Residues with variations found in the Alpha, Beta and delta variants were visualized on this structure with the Visual Molecular Dynamics program (Humphrey et al., 1996).

1　zhanggroup.org/COVID-19

Results

RNA-seq demonstrates RK-33 treatment downregulates multiple viral transcripts and alters the host transcriptional landscape
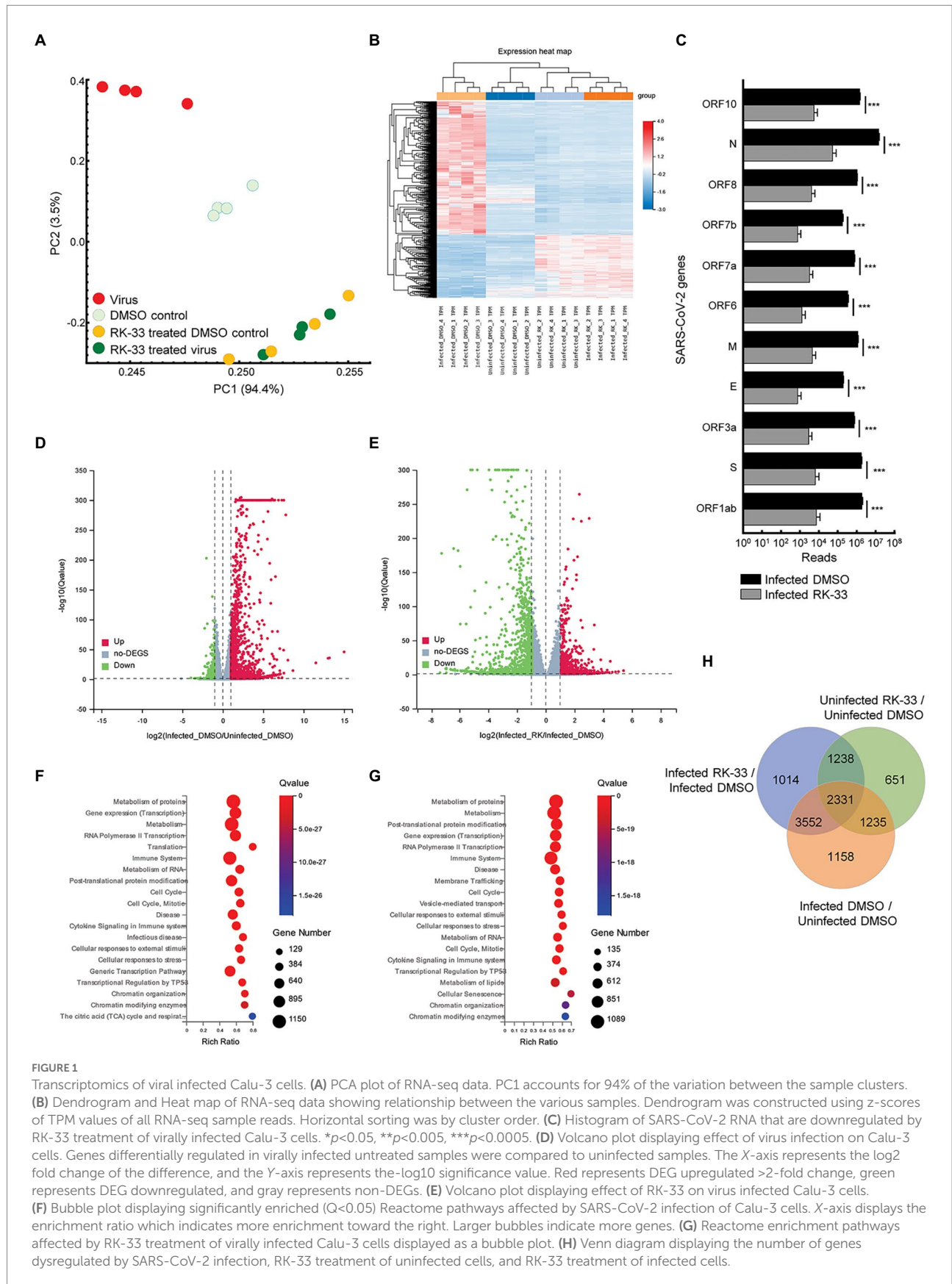
To study the effect of RK-33 and SARS-CoV-2 on the human transcriptome, we performed RNA-seq on isolated RNA from uninfected Calu-3 cells treated with DMSO (DMSO control), cells treated with RK-33 (RK-33 treated DMSO control), cells infected with SARS-CoV-2 and treated with DMSO (Virus), and cells infected with SARS-CoV-2 and treated with RK-33 (RK-33 treated virus). A non-toxic dose of RK-33 ($5\,\mu M$) was used for these studies and cells were infected at a MOI of 0.1. All samples were collected at 48 hpi. RNA-Seq was mapped separately to human genome and SARS-CoV-2 genome. Principal Components Analysis (PCA) of host RNA showed a good separation between the infected samples and the control treated samples, while the RK-33 treated samples were clustered together. As expected, RK-33 and SARS-CoV-2 infection were the drivers for sample segregation (Figure 1A; Supplementary Figure S1). Hierarchical clustering separated all RNA samples according to treatment with the viral infected cells being the most different compared to the other three groups (Figure 1B). RNA of most SARS-CoV-2 genes (ORF1ab, S, ORF3a, E, M, ORF7a, ORF7b, ORF8, N, ORF10) exhibited a reduction when treated with RK-33 compared to virus infected control cells (Figure 1C). Volcano plots were produced to compare host RNA expression between RK-33 treated, viral infected cells and untreated, viral infected cells (Figure 1D). We also compared effects of viral infection on untreated Calu-3 cells (Figure 1E). Many of the genes that were upregulated by the virus were significantly downregulated by RK-33 treatment. We studied genes that were significantly dysregulated (>1.1 FC, $p < 0.05$) by RK-33 treatment of virally infected Calu-3 cells (Infected RK-33 vs. Infected DMSO), by virus infection of the cells (Infected DMSO vs. Uninfected DMSO), and with the control (Uninfected RK-33 vs. Uninfected DMSO). The gene sets were plotted on a Venn diagram (Figure 1F), and show the largest overlap exists between the RK-33 treated virally infected cells and the virally infected cells, indicating the widespread effects of SARS-CoV-2 on the genetic landscape. Reactome pathway analysis (Fabregat et al., 2017; Jassal et al., 2020) revealed that the top five pathways enriched in viral infected DMSO treated control cells were Metabolism of proteins, Gene expression (transcription), Metabolism, RNA Pol II transcription, and Translation (Figure 1G). The top five Reactome pathways enriched in viral infected RK-33 treated cells were Metabolism of proteins, Metabolism, Post-translational protein modification, Gene expression (transcription), and RNA Pol II transcription (Figure 1H). It is important to note that host translation is less significantly impacted after cells are treated with RK-33. Gene set enrichment
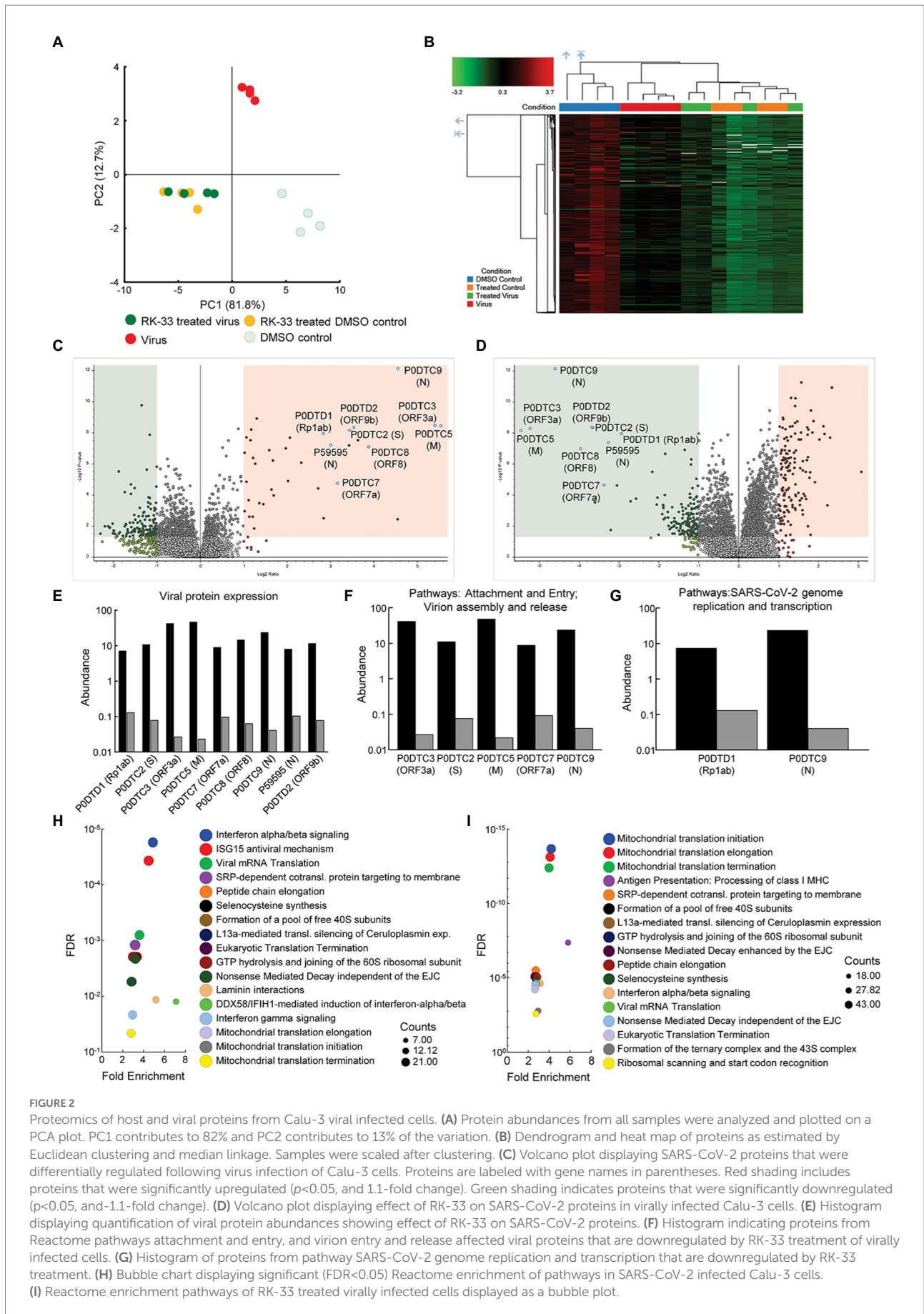
analysis of the uninfected cells and RK-33 treated virus infected cells are shown in Supplementary Figures S2, S3. Analysis of genes dysregulated by SARS-CoV-2 infection and RK-33 treatment expectedly showed a larger effect (Supplementary Figure S3). We also compared our gene set with published data (Blanco-Melo et al., 2020) which showed a large commonality both in Calu-3 gene sets and in the deceased COVID-19 lung tissue set (Supplementary Figure S4). In addition, RNA-seq QC results indicated that all samples had around 45 million clean reads, but alignment QC indicated SARS-CoV-2 infected Calu-3 cells had around 33% unique matches in the human genome compared to the rest of the samples at 88% (Supplementary Figure S5). This is an important result, as it is known that the Nsp1 degrades host RNA so that it can hijack the host cell (Huang et al., 2011). This reversion of viral to host RNA in the RK-33 treated SARS-CoV-2 infected cells demonstrates the role of DDX3 in SARS-CoV-2 replication and the importance of targeting DDX3 by RK-33.

Proteomics analysis indicated RK-33 treatment suppresses multiple viral proteins and alters the host response to infection

To study changes in the human and viral proteome after infection with SARS-CoV-2 and RK-33 treatment, we performed proteomics analysis on SARS-CoV-2 infected Calu-3 cells treated with DMSO solvent control (Virus) and on the RK-33 treated and virus infected Calu-3 cells (RK-33 treated virus) as described above. Other controls used were uninfected Calu-3 cells treated with RK-33 (RK-33 treated DMSO control) and Calu-3 cells treated with DMSO (DMSO control). PCA showed clear separation between virally infected and uninfected cells as well as virally infected cells treated with DMSO, and virally infected cells treated with RK-33 (Figure 2A; Supplementary Figure S6). This indicated that RK-33 and viral infection were the major factors driving the segregation of samples on the PCA plot. Next, we determined the clustering pattern of the untreated and RK-33 treated host cells following virus infection. As shown in the dendrogram and heat map (Figure 2B; Supplementary Figure S7), the virus infected Calu-3 samples and the uninfected samples clustered separately while the RK-33 treated virus infected samples as well as uninfected RK-33 samples clustered among each other.

To study how RK-33 treatment affected Calu-3 infected cells, we plotted the data using Volcano plots (Figures 2C, D). As expected, most of the SARS-CoV-2 proteins (P0DTC2 spike glycoprotein, P0DTC3 ORF3a, P0DTC5 membrane protein, P0DTC8 ORF8, P0DTC9 nucleoprotein, P0DTD1 replicase polyprotein 1ab, P0DTD2 ORF9b, P59595 nucleoprotein) were significantly upregulated (>7.5 FC) after infection of Calu-3 cells. RK-33 treatment significantly downregulated (>8 FC) all these viral proteins in Calu-3 cells. Changes in protein abundance are displayed in Figures 2E–G.

FIGURE 1

Transcriptomics of viral infected Calu-3 cells. **(A)** PCA plot of RNA-seq data. PC1 accounts for 94% of the variation between the sample clusters. **(B)** Dendrogram and Heat map of RNA-seq data showing relationship between the various samples. Dendrogram was constructed using z-scores of TPM values of all RNA-seq sample reads. Horizontal sorting was by cluster order. **(C)** Histogram of SARS-CoV-2 RNA that are downregulated by RK-33 treatment of virally infected Calu-3 cells. *$p < 0.05$, **$p < 0.005$, ***$p < 0.0005$. **(D)** Volcano plot displaying effect of virus infection on Calu-3 cells. Genes differentially regulated in virally infected untreated samples were compared to uninfected samples. The *X*-axis represents the log2 fold change of the difference, and the *Y*-axis represents the -log10 significance value. Red represents DEG upregulated >2-fold change, green represents DEG downregulated, and gray represents non-DEGs. **(E)** Volcano plot displaying effect of RK-33 on virus infected Calu-3 cells. **(F)** Bubble plot displaying significantly enriched (Q<0.05) Reactome pathways affected by SARS-CoV-2 infection of Calu-3 cells. *X*-axis displays the enrichment ratio which indicates more enrichment toward the right. Larger bubbles indicate more genes. **(G)** Reactome enrichment pathways affected by RK-33 treatment of virally infected Calu-3 cells displayed as a bubble plot. **(H)** Venn diagram displaying the number of genes dysregulated by SARS-CoV-2 infection, RK-33 treatment of uninfected cells, and RK-33 treatment of infected cells.

FIGURE 2
Proteomics of host and viral proteins from Calu-3 viral infected cells. **(A)** Protein abundances from all samples were analyzed and plotted on a PCA plot. PC1 contributes to 82% and PC2 contributes to 13% of the variation. **(B)** Dendrogram and heat map of proteins as estimated by Euclidean clustering and median linkage. Samples were scaled after clustering. **(C)** Volcano plot displaying SARS-CoV-2 proteins that were differentially regulated following virus infection of Calu-3 cells. Proteins are labeled with gene names in parentheses. Red shading includes proteins that were significantly upregulated ($p<0.05$, and 1.1-fold change). Green shading indicates proteins that were significantly downregulated ($p<0.05$, and -1.1-fold change). **(D)** Volcano plot displaying effect of RK-33 on SARS-CoV-2 proteins in virally infected Calu-3 cells. **(E)** Histogram displaying quantification of viral protein abundances showing effect of RK-33 on SARS-CoV-2 proteins. **(F)** Histogram indicating proteins from Reactome pathways attachment and entry, and virion entry and release affected viral proteins that are downregulated by RK-33 treatment of virally infected cells. **(G)** Histogram of proteins from pathway SARS-CoV-2 genome replication and transcription that are downregulated by RK-33 treatment. **(H)** Bubble chart displaying significant (FDR<0.05) Reactome enrichment of pathways in SARS-CoV-2 infected Calu-3 cells. **(I)** Reactome enrichment pathways of RK-33 treated virally infected cells displayed as a bubble plot.

Subsequently, we performed pathway analysis using Reactome to compare RK-33 treated infected cells with control infected cells. The five most significant pathways that were enriched following SARS-CoV-2 infection were interferon alpha/beta signaling, ISG15 antiviral mechanism, viral mRNA translation, SRP-dependent cotranslational protein targeting to membrane, and peptide chain elongation (Figure 2H). In contrast, RK-33 treatment of SARS-CoV-2 infected cells results in a shift of pathways being impacted, with the five most significant pathways enriched being Mitochondrial translational initiation, Mitochondrial translational elongation, Mitochondrial translational termination, Antigen Presentation: Folding, assembly and peptide loading of class I MHC, and SRP-dependent cotranslational protein targeting to membrane (Figure 2I). We also queried the STRING database (Szklarczyk et al., 2019) and found pathways in RK-33 treated cells that were positively enriched (Endosomal/vacuolar pathway and Regulation of Complement cascade) and negatively enriched (Mitochondrial translation and Mitochondrial translation initiation). Pathways in virus infected DMSO control cells that were positively enriched included Regulation of IFNA signaling and Interferon alpha/beta signaling while Translation of Replicase and replication transcription complex and Endosomal sorting complex required for transport were negatively enriched (Supplementary Figure S8). These data indicate that RK-33 treatment suppresses viral protein production corresponding to changes in the host proteomic landscape especially as it relates to innate immune response pathways.

RK-33 inhibits HCoV-OC43 and SARS-CoV-2 production

Given that DDX3 has been shown to play a regulatory role in the viral biogenesis, we initially tested the impact of RK-33 on coronavirus replication using human coronavirus OC43 (betacoronavirus) as a BSL-2 model of SARS-CoV-2. The CC50 value of RK-33 on Rhabdomyosarcoma (RD) muscle cells (highly susceptible to HCoV-OC43 infection), was determined to be 3.22 μM (Figure 3A). Next the antiviral impact of RK-33 was tested on RD cells using non-toxic concentrations of RK-33 (0.1 and 1 μM). Treatment with 1 μM of RK-33 decreased HCoV-OC43 infectious titers by over 100-fold (> ~2 logs; Figure 3B). As can be seen in Figure 3C, HCoV-OC43 infection of RD cells results in extensive cytopathic effect (CPE) by 4 dpi (left panel) that was partially relieved by 1 μM of RK-33 treatment (right panel). These data indicate that RK-33 is effective against a betacoronavirus, which encouraged us to test its impact on SARS-CoV-2.

Thus, since in our study we used Calu-3 cells (lung cancer cell line) as a model cell line for SARS-CoV-2 infection, our initial step in antiviral testing was to establish the CC50 of RK-33 in Calu-3 cells. For this purpose, cells were incubated with RK-33 in concentrations ranging from 0.39-50 μM for 24 h. Cell viability was measured by CellTiter-Glo assay which measures ATP production. The established CC50 for Calu-3 cell lines was 13.48 μM (Figure 3D). Next, the EC50 of RK-33 against SARS-CoV-2 was

determined by treatment of Calu-3 cells with 0.31–5 μM RK-33 or 0.05% DMSO for 24 h prior to infection. RK-33 and DMSO treated cells were infected with SARS-CoV-2 Washington isolate (Lineage A) at an MOI of 0.1 and 48 hpi the amount of infectious virus in the supernatants was determined by plaque assay. Overall, RK-33 displayed potent anti-SARS-CoV-2 effect on Calu-3 cells with an $EC_{50} < 1 \mu M$ (Figure 3E), resulting in a selectivity index (CC50/EC50) of 14.5. To confirm these results, a similar experiment was performed with cells treated with DMSO or 5 μM RK-33. In agreement with the results in Figure 3E, RK-33 treatment had a significant three log reduction in SARS-CoV-2 viral titers (Figure 3F) RK-33 treatment also resulted in a reduction of ~2.5–3 log10 of intracellular viral RNA production as measured by RT-qPCR analysis using primers recognizing RdRp and E genes/regions (Figure 3G). Finally, a one log reduction in extracellular viral RNA (from cell-free supernatants) was also observed (Figure 3H) in RK-33 treated samples.

Mutation status of SARS-CoV-2 proteins

Along with its worldwide spread, SARS-CoV-2 virus has mutated resulting in genome-wide amino acid variations across the four variants of varying lineages as displayed in Figure 4A. Protein N in the Alpha and Delta variants shows greater divergence from Lineage A than the spike proteins of these same variants. Proteins E, nsp7, and ORF3a have diverged more than the spike in the Beta variant, and the Delta variant displays some level of divergence from Lineage A in the M, nsp2, nsp4, nsp6, and NendU proteins. Due to large deletions and a frameshift, the ORF8 protein in the Delta variant has diverged from Lineage A to a greater extent than spike protein[2] (Supplementary Table 1). Furthermore, Figure 4B displays amino acid substitutions and deletions with respect to the Lineage A variant in sixteen of the proteins. This includes large truncations in ORF7a (Beta and Delta variants) and ORF8 (Alpha variant) and a high number of variations in the hACE2 receptor-interfacing spike proteins. Spike protein amino acid substitutions and deletions with respect to Lineage A variant are further visualized along the protein sequence at higher resolution in Figure 4C. These variations occur throughout the spike protein molecular structure, including within the S1-receptor-binding-domain as seen in the 3D models in Figure 4D. Details of mutations can be found in Supplementary Table 1.

RK-33 inhibits Alpha, Beta, and Delta variants of SARS-CoV-2

Due to the diversity between different viral variants, we next tested the effect of RK-33 on replication and virion production of different of SARS-CoV-2 variants. RK-33 treatment of cells resulted in a significant reduction (2–4 log fold) of infectious
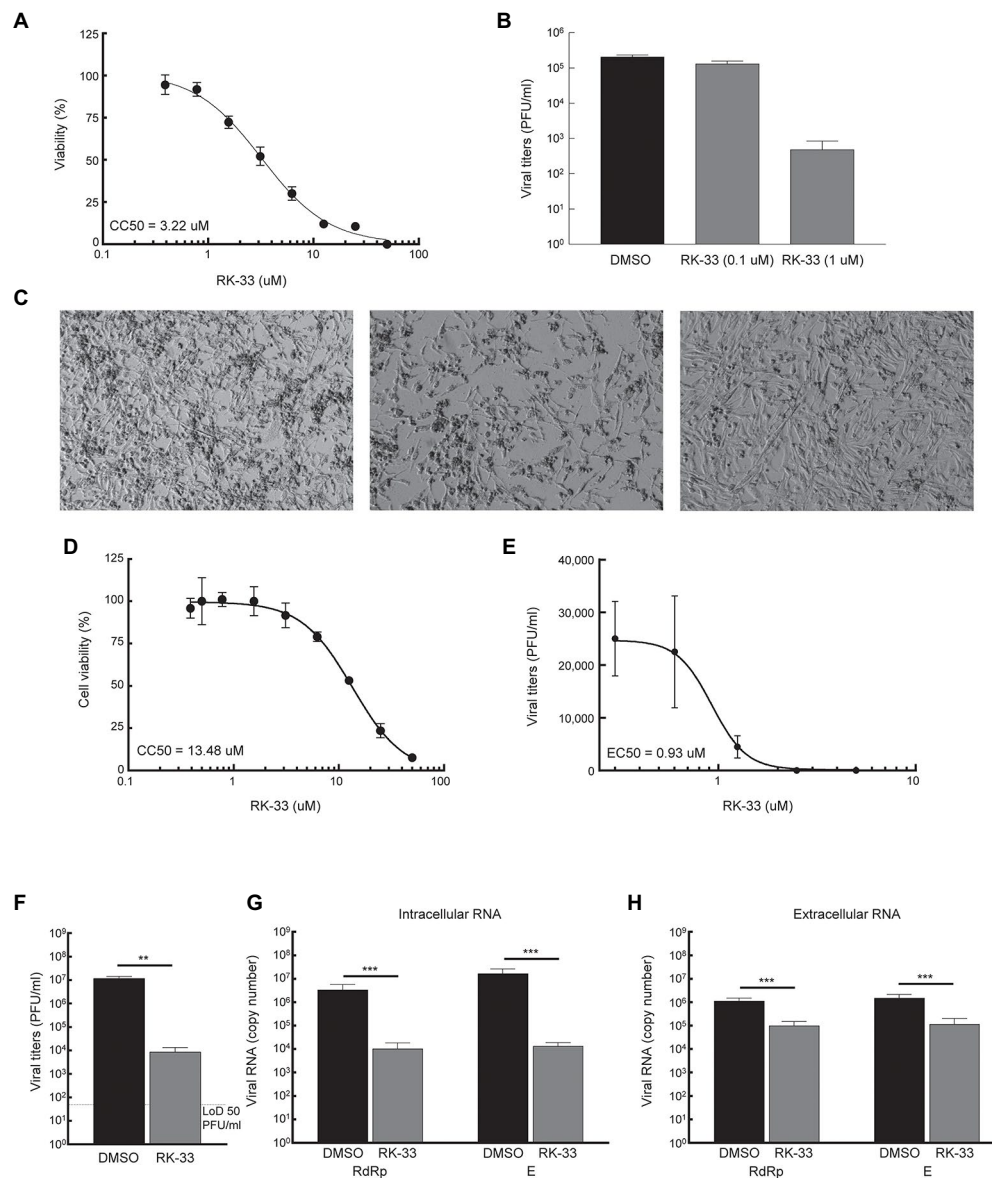
---

2 https://covariants.org/

FIGURE 3

RK-33 decreases production of hCoV-OC43 and SARS-CoV-2. **(A)** RD cells were treated with various concentrations of RK-33 and cell viability determined post-treatment using CellTiter Glo assay. **(B)** RD cells were treated with RK-33 for 1 h followed by infection with hCoV-OC43 (MOI 0.1) and infectious titers at 3 dpi were determined *via* plaque assay. **(C)** RD cells were treated with RK-33 for 1 h followed by infection with hCoV-OC43 (MOI 0.1). CPE was observed at 4 dpi. **(D)** Calu-3 cells were treated with various concentrations of RK-33 and cell viability determined using CellTiter Glo assay. **(E)** Calu-3 cells were treated with various concentrations of RK-33 for 24 h followed by infection with SARS-CoV-2 Washington Variant (Lineage A; MOI 0.1) in the presence of RK-33. Cells were also post-treated with RK-33. Supernatants were collected at 48 hpi and plaque assays performed to determine infectious titers. DMSO was included as a negative control. **(F)** Calu-3 cells were treated with RK-33 (5 μM) or DMSO as described in panel **E** and viral titers determined by plaque assay. **(G,H)** Intra and extra cellular SARS-CoV-2 RNA viral copy numbers as measured by RT-qPCR of RdRp and E genes. Data represents the average of 3 biological replicates and error bars display standard deviations. *$p<0.05$, **$p<0.005$, ***$p<0.0005$.

titers of the Alpha, Beta, and Delta variants (Figure 5A). Analysis of the intracellular and extracellular RNA (RdRp and E genes) also showed significant difference between RK-33 treated and DMSO control samples in the amount of the viral RNA production (Figures 5B–G). In conclusion, RK-33 displayed potent antagonistic SARS-CoV-2 effects against all tested variants.

RK-33 effects TMPRSS2 and reduces spike-pseudotyped lentivirus constructs *in vitro*

The transmembrane serine protease TMPRSS2 has been identified as the protease that cleaves spike protein of SARS-CoV-2 thus facilitating entry (Hoffmann et al., 2020). To determine if
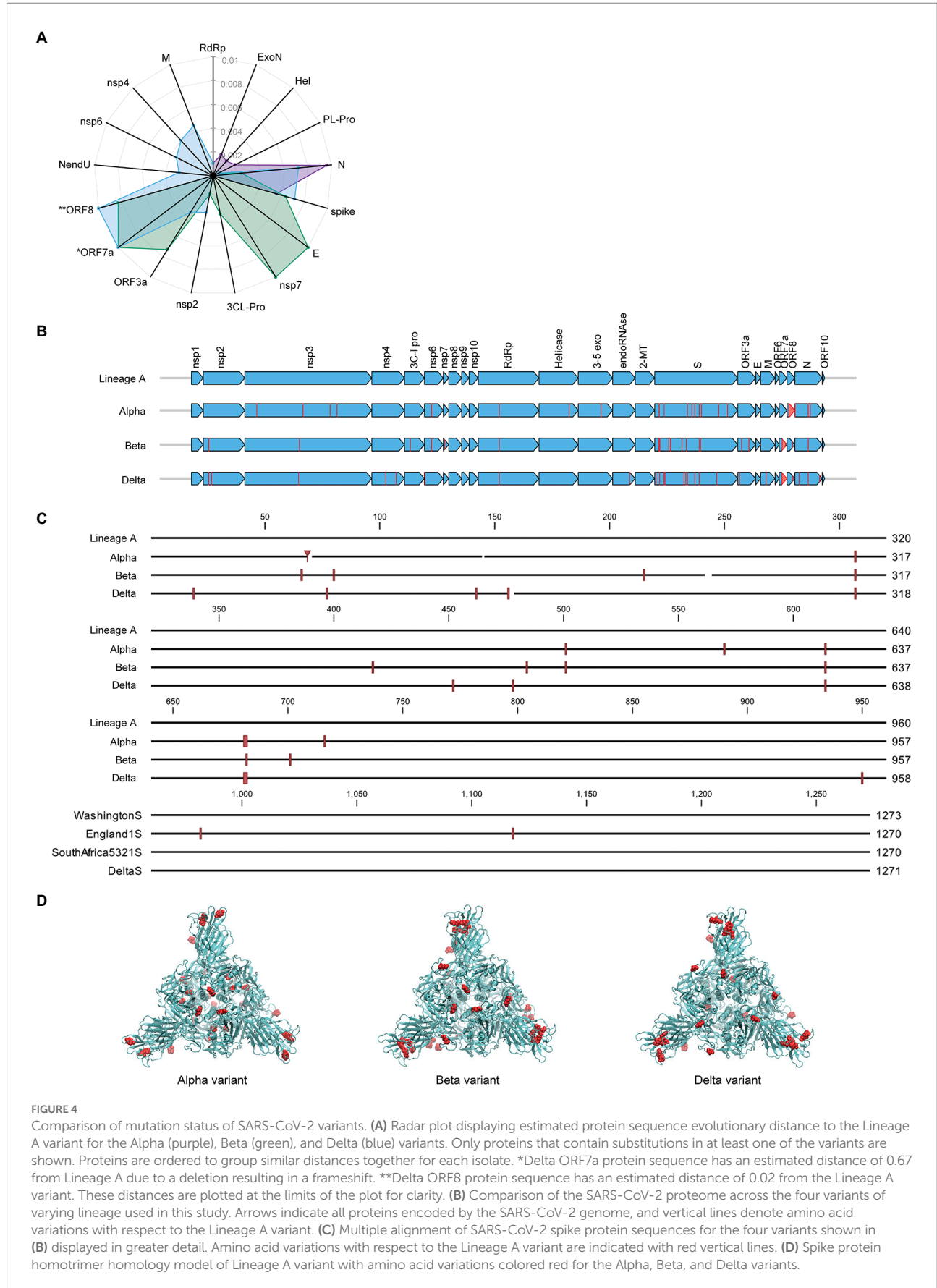
FIGURE 4
Comparison of mutation status of SARS-CoV-2 variants. **(A)** Radar plot displaying estimated protein sequence evolutionary distance to the Lineage A variant for the Alpha (purple), Beta (green), and Delta (blue) variants. Only proteins that contain substitutions in at least one of the variants are shown. Proteins are ordered to group similar distances together for each isolate. *Delta ORF7a protein sequence has an estimated distance of 0.67 from Lineage A due to a deletion resulting in a frameshift. **Delta ORF8 protein sequence has an estimated distance of 0.02 from the Lineage A variant. These distances are plotted at the limits of the plot for clarity. **(B)** Comparison of the SARS-CoV-2 proteome across the four variants of varying lineage used in this study. Arrows indicate all proteins encoded by the SARS-CoV-2 genome, and vertical lines denote amino acid variations with respect to the Lineage A variant. **(C)** Multiple alignment of SARS-CoV-2 spike protein sequences for the four variants shown in **(B)** displayed in greater detail. Amino acid variations with respect to the Lineage A variant are indicated with red vertical lines. **(D)** Spike protein homotrimer homology model of Lineage A variant with amino acid variations colored red for the Alpha, Beta, and Delta variants.

abrogating DDX3 activity by RK-33 would affect TMPRSS2 expression, we treated Calu-3 cells with increasing concentrations of RK-33 for 48 h and probed for the levels of TMPRSS2 and DDX3 by immunoblotting. As shown in Figure 6A, RK-33 (5 µM) was able to reduce TMPRSS2 expression by 50% in 48 h (Fiji / ImageJ). To determine if the decrease in TMPRSS2 level by RK-33 had any biological significance on viral entry, we treated Calu-3 cells with RK-33 for 24 h, followed by infection with a SARS-CoV-2 Spike-pseudotyped GFP lentivirus construct. Two days following infection, we counted the GFP cells using a random unbiased approach. As shown in Figure 6B, use of RK-33 at CC5 (3 µM), reduced the infected cell numbers by 50%. This supports our hypothesis that dysregulating DDX3 by RK-33 can affect TMPRSS2 expression resulting in decrease in SARS-CoV-2 lentivirus infection of Calu-3 cells.

Discussion

SARS-CoV-2 has been successfully targeted in a few ways. Prophylactic vaccines are available that reduce/eliminate hospitalization and associated medical complications due to COVID-19. Presently, other treatments are limited to the antiviral nucleoside analog Remdesivir from Gilead Biosciences and a monoclonal antibody cocktail from Regeneron. However, Remdesivir is only prescribed in severe cases, and both require intravenous infusion making it difficult to obtain without hospitalization. Moreover, Remdesivir has shown mixed results in reducing the time to recovery in hospitalized patients (Beigel et al., 2020; Malin et al., 2020; Spinner et al., 2020; Wang et al., 2020; Garibaldi et al., 2021). Another nucleoside analog drug Molnupiravir from Merck reduces the risk of hospital admission or death by approximately 50% in patients at risk for poor outcomes (Mahase, 2021).

On the other hand, identifying virus-host interacting factors could reveal new targets to mitigate medical complications associated with SARS-CoV-2 infection. Over the years, several roles of a host protein, DDX3, have been identified as crucial for replication and production of many viruses (Squeglia et al., 2020; Ciccosanti et al., 2021). Interestingly, DDX3 has also been identified, using proteomics, to be involved in SARS-CoV-2 replication (Squeglia et al., 2020; Ciccosanti et al., 2021). Moreover, computational and system biology approaches have indicated different proteins of SARS-CoV-2 to be associated with cellular organelle functions that are regulated by DDX3 activity (Gordon et al., 2020a). In this study, we used a small molecule inhibitor of DDX3, RK-33, to study its impact of SARS-CoV-2. Using the Lineage A variant, we showed that RK-33 reduced viral titers by over 10,000-fold by plaque assay. These data were further validated by RT-qPCR (RdRp and envelope) of the intra-and extracellular SARS-CoV-2 RNA of the RK-33 treated Lineage A infected Calu-3 cells. This work is in agreement with a study showing that inhibition of DDX3 by two different DDX3 inhibitors, RK-33 and C-4B, impacted SARS-CoV-2 RNA production, but this study did not determine the impact on viral titers by plaque assay (Ciccosanti et al., 2021).

Based on this encouraging finding, we performed RNA-seq and proteomics analysis on SARS-CoV-2 infected Calu-3 cells, before and after RK-33 treatment. PCA of the RNA showed the major effect of RK-33 on the cells. It was interesting to note that in the virus infected Calu-3 cells, more than 80% of the RNA species was that of SARS-CoV-2, while in the RK-33 group, the host mRNA species was 80% represented. This is indicative that perturbing DDX3 by RK-33 restored many of the host cellular functions while suppressing SARS-CoV-2 replication. This could be clearly seen in both the heat map and the PCA plot with RK-33 treatment serving to "normalize" expression of the virus infected cells toward the uninfected cell type gene expression. Volcano plots also demonstrated how the high gene expression patterns caused by the virus infection were modulated by RK-33 treatment of the cells. The sensitivity of RK-33 to reduce Lineage A titers is indicative of the potential of targeting host proteins for SARS-CoV-2 treatment.

To further characterize the effect of RK-33 on the host cellular machineries, we performed proteomics on SARS-CoV-2 infected Calu-3 cells. Proteomic-based PCA analysis showed that RK-33 treated virus infected samples segregated from the untreated infected samples. The results indicated that RK-33 was the major determinant of segregation in the PCA plot. Subsequent pathway analysis showed that many of the downregulated pathways were associated with virus attachment, entry, assemble and release. Proteomics analysis clearly demonstrated that most of the proteins involved in SARS-CoV-2 genome replication and transcription (ORF1 ab, ORF3A, Spike, Membrane, ORF7A and Nucleoprotein) were significantly downregulated by RK-33 in SARS-CoV-2 infected Calu-3 cells. The ability of RK-33 to reduce viral titers of SARS-CoV-2 Lineage A could reflect on the dependence of SARS-CoV-2 on DDX3 for its replication. This is probably because at the molecular level SARS-CoV-2 usurps DDX3 in the host cell to its advantage for replication and for pathogenesis. This is in parallel to what is already demonstrated by many other viruses that utilize DDX3 for viral entry, processing, and egress from the host cells (Winnard et al., 2021). Furthermore, as DDX3 has been shown to interact with nucleocapsid protein of SARS-CoV-2 (Ciccosanti et al., 2021), it is plausible that the use of RK-33 is directly interfering with SARS-CoV-2 replication machinery as well.

Based on these promising results, we evaluated the effect of RK-33 on viral titers in the Alpha, Beta, and Delta variant-infected cells. RK-33 was able to reduce the viral loads by 2-3 log folds. This is not unexpected as targeting host factors essential for viral replication, such as DDX3, would have similar outcomes for all the variants. As is evident from the spike protein modeling, there is a higher concentration of spike protein mutation within the ACE-2 binding region, but this does not affect the ability of RK-33 to reduce viral titers across all the variants. Also, the amino acid substitutions lead to increased evolutionary distances in different proteins among the four isolates used in this study. Thus, the four variants used in this study could serve as diverse models adapted to provide a growth advantage or independent evolution of SARS-CoV-2 leading to increased virulence and pathogenesis.
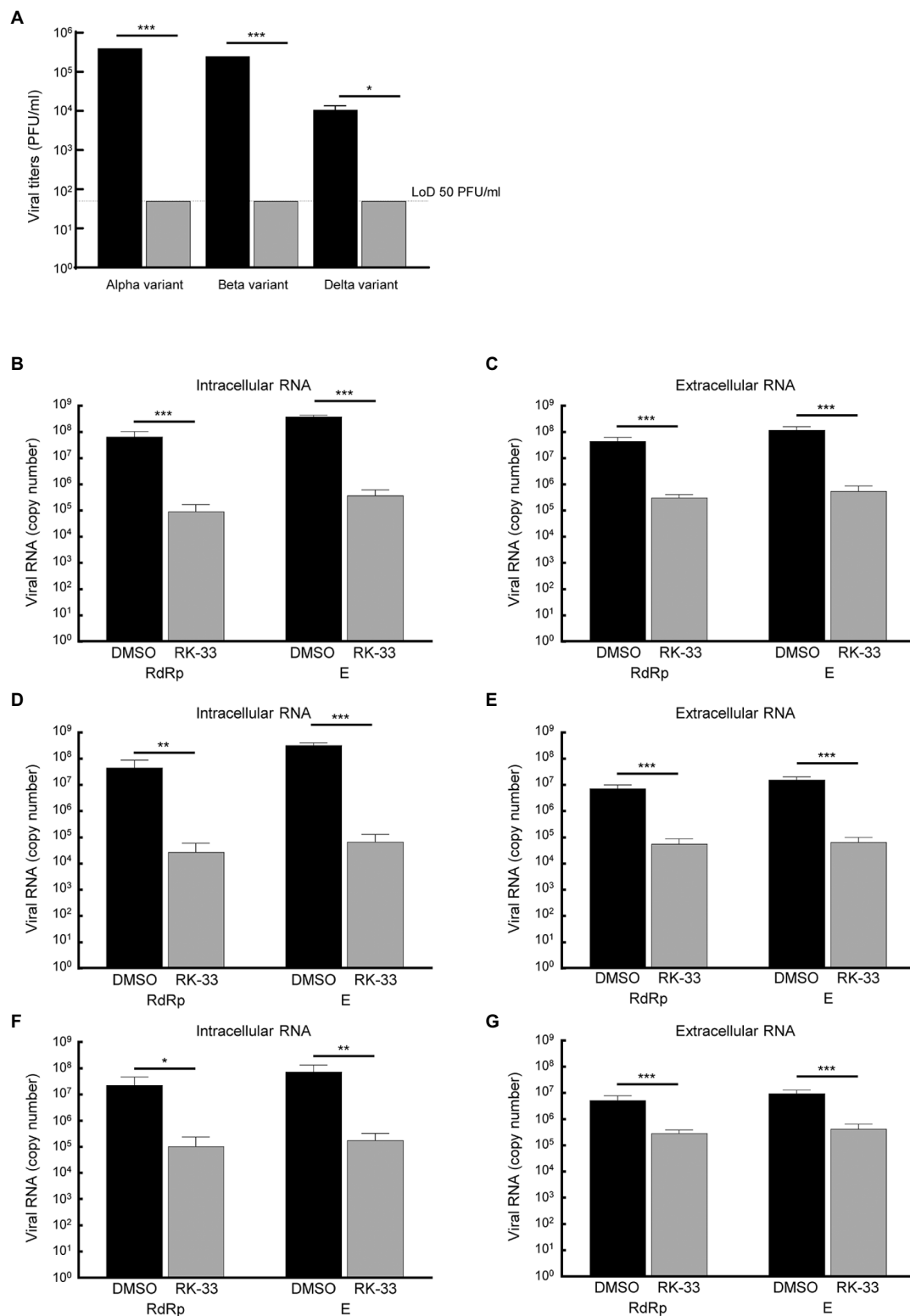
FIGURE 5

(A) Calu-3 cells were treated with RK-33 (5uM) for 24 h followed by infection with Alpha, Beta, and Delta variants of SARS-CoV-2. Supernatants were collected at 48 hpi and plaque assays performed to determine infectious titers. DMSO was included as a negative control. **(B)** RNA was extracted from SARS-CoV-2 Alpha variant-infected cells treated with RK-33 and subjected to RT-qPCR in a one-step protocol that amplified RdRp and E genes. Copy numbers were calculated from known positive controls. **(C)** Extracellular RNA was extracted from above cell supernatants and processed as earlier. **(D,E)** Results from intra-and extracellular RNA from RK-33 treatment of Beta variant infection. **(F,G)** Results from intra and extracellular RNA from RK-33 treatment of Delta variant. $*p<0.05$, $**p<0.005$, $***p<0.0005$.
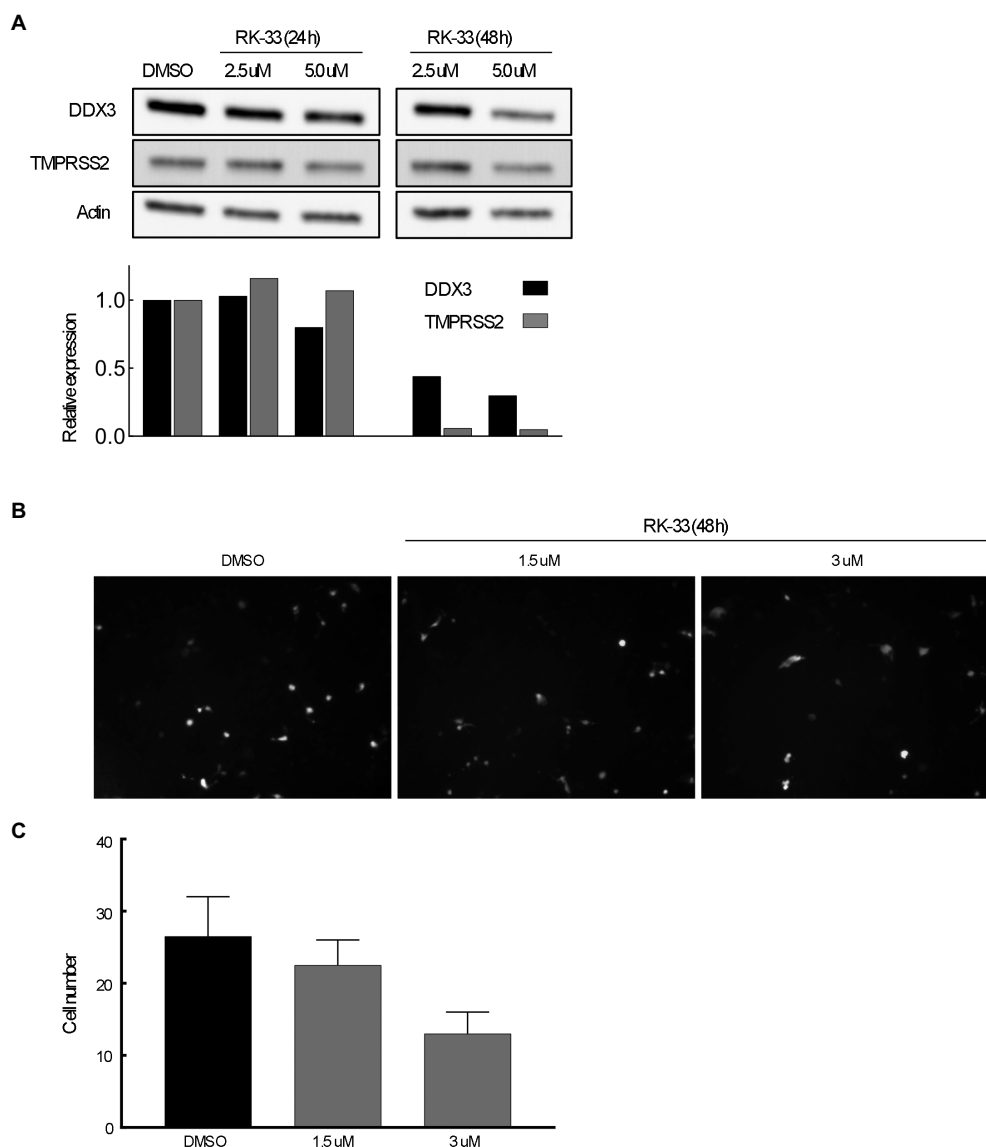
FIGURE 6
(A) Immunoblot of proteins extracted from Calu-3 cells treated with increasing concentrations of RK-33 for 24 and 48 h. Densitometry graph included. **(B)** Effect of increasing concentrations of RK-33 on Calu-3 cells for 48 h that were infected with pseudotyped virus. **(C)** Quantification of Calu-3 cells seen in **(B)**.

Furthermore, we showed that RK-33 was able to reduce TMPRSS2 expression in Calu-3 cells. A key aspect of the TMPRSS2 gene is the presence of guanine-rich tracts of DNA in its gene promoter that can form G-quadruplex structures. These structures can be targeted by benzoselenoxanthene derivatives that stabilize TMPRSS2 G-quadruplexes *in vitro*, thus downregulating TMPRSS2 gene expression (Shen et al., 2020). In this context, DDX3 was found to facilitate both translation of general complex secondary structures including G-quadruplexes (Lai et al., 2008, 2010), as well as mRNAs with secondary structure in immediate vicinity to their m⁷GTP cap (Soto-Rifo et al., 2012). We have presented data that demonstrates that use of RK-33 even at CC5, reduced the SARS-CoV-2 infection rate by 50%. In

support of our findings, a recent paper by Liu et al. (2022) demonstrated that the use of G-quadruplex specific stabilizers could reduce SAR-CoV-2 infection in a pseudovirus cell system and in mouse models.

These data indicate that targeting DDX3 by RK-33 for SARS-CoV-2 treatment could potentially reduce SARS-CoV-2 virulence and pathogenicity by two different mechanisms. First, it can decrease the infection rate by downregulating TMPRSS2 protein expression, and second, reduce the pathogenicity, by suppressing SARS-CoV-2 replication. This two-prong mechanism of action would be extremely effective at suppressing viral replication of any newly emerging variants of concern, which is in line with an antiviral that is targeting a host

factor. We fully appreciate that the impact of RK-33 on TMRPSS2 expression is only one mechanism by which RK-33 may be impacting SARS-CoV-2 production. Indeed, our proteomic and transcriptomic analysis points to multiple cellular events being altered in infected cells by RK-33 treatment, such as innate immune responses, translation, and membrane trafficking, each of which are important for viral production.

In conclusion, we report on the importance of DDX3 and its targeting by the small molecule inhibitor RK-33 which was developed earlier by rational drug design that resulted in a unique structural scaffold with little or no toxicity in animals (Kondaskar et al., 2010; Bol et al., 2015; Xie et al., 2016; Heerma van Voss et al., 2018). Use of RK-33 on Calu-3 cells resulted in suppressing virus titers from all four isolates and has the potential to treat SARS-CoV-2 infection. We are the first to present a promising HTA strategy to tackle the different variants associated with SARS-CoV-2 as well as subsequent variants that may arise.

Author's note

The following SARS-CoV-2 isolates were obtained through BEI Resources, NIAID, NIH: SARS-Related Coronavirus 2, Isolate USA-WA1/2020, NR-52281, SARS-Related Coronavirus 2, Isolate hCoV-19/South Africa/KRISP-EC-K005321/2020, NR-54008, contributed by Alex Sigal and Tulio de Oliveira, SARS-Related Coronavirus 2, Isolate hCoV-19/England/204820464/2020, NR-54000, contributed by Bassam Hallis, SARS-Related Coronavirus 2, Isolate hCoV-19/USA/PHC658/2021 (Lineage B.1.617.2; Delta Variant), NR-55611, contributed by Richard Webby and Anami Patel. Pseudotyped viruses were a kind gift from Prashant Desai (Department of Oncology, Sidney Kimmel Comprehensive Cancer Center, Baltimore, MD, United States).

Data availability statement

The data presented in the study are deposited in the Gene Expression Omnibus (GEO) repository, accession number GSE209800.

Author contributions

FV, IA, KK-H, and VR planned the experiments and analyzed the results. FV, IA, PW, S-CL, and LP performed the experiments. FV, IA, PW, K-KH, and VR wrote the manuscript. All authors contributed to the article and approved the submitted version.

Conflict of interest

VR holds a patent on the composition of RK-33 (US patent # 8518901).

The remaining authors declare that the research was conducted in the absence of any commercial or financial relationships that could be construed as a potential conflict of interest.

Publisher's note

All claims expressed in this article are solely those of the authors and do not necessarily represent those of their affiliated organizations, or those of the publisher, the editors and the reviewers. Any product that may be evaluated in this article, or claim that may be made by its manufacturer, is not guaranteed or endorsed by the publisher.

Supplementary material

The Supplementary Material for this article can be found online at: https://www.frontiersin.org/articles/10.3389/fmicb.2022.959577/full#supplementary-material

References

Baughn, L. B., Sharma, N., Elhaik, E., Sekulic, A., Bryce, A. H., and Fonseca, R. (2020). Targeting TMPRSS2 in SARS-CoV-2 infection. *Mayo Clin. Proc.* 95, 1989–1999. doi: 10.1016/j.mayocp.2020.06.018

Beigel, J. H., Tomashek, K. M., Dodd, L. E., Mehta, A. K., Zingman, B. S., Kalil, A. C., et al. (2020). Remdesivir for the treatment of Covid-19 - final report. *N. Engl. J. Med.* 383, 1813–1826. doi: 10.1056/NEJMoa2007764

Blanco-Melo, D., Nilsson-Payant, B. E., Liu, W. C., Uhl, S., Hoagland, D., Møller, R., et al. (2020). Imbalanced host response to SARS-CoV-2 drives development of COVID-19. *Cell* 181:e1039, 1036–1045. doi: 10.1016/j. cell.2020.04.026

Bol, G. M., Vesuna, F., Xie, M., Zeng, J., Aziz, K., Gandhi, N., et al. (2015). Targeting DDX3 with a small molecule inhibitor for lung cancer therapy. *EMBO Mol. Med.* 7, 648–669. doi: 10.15252/emmm.201404368

Brai, A., Boccuto, A., Monti, M., Marchi, S., Vicenti, I., Saladini, F., et al. (2020a). Exploring the implication of DDX3X in DENV infection: discovery of the first-in-class DDX3X fluorescent inhibitor. *ACS Med. Chem. Lett.* 11, 956–962. doi: 10.1021/acsmedchemlett.9b00681

Brai, A., Fazi, R., Tintori, C., Zamperini, C., Bugli, F., Sanguinetti, M., et al. (2016). Human DDX3 protein is a valuable target to develop broad spectrum antiviral agents. *Proc. Natl. Acad. Sci. U. S. A.* 113, 5388–5393. doi: 10.1073/pnas.1522987113

Brai, A., Martelli, F., Riva, V., Garbelli, A., Fazi, R., Zamperini, C., et al. (2019a). DDX3X helicase inhibitors as a new strategy to fight the West Nile virus infection. *J. Med. Chem.* 62, 2333–2347. doi: 10.1021/acs.jmedchem.8b01403

Brai, A., Riva, V., Saladini, F., Zamperini, C., Trivisani, C. I., Garbelli, A., et al. (2020b). DDX3X inhibitors, an effective way to overcome HIV-1 resistance targeting host proteins. *Eur. J. Med. Chem.* 200:112319. doi: 10.1016/j.ejmech.2020.112319

Brai, A., Ronzini, S., Riva, V., Botta, L., Zamperini, C., Borgini, M., et al. (2019b). Synthesis and antiviral activity of novel 1,3,4-Thiadiazole inhibitors of DDX3X. *Molecules* 24:13988. doi: 10.3390/molecules24213988

Cencic, R., Desforges, M., Hall, D. R., Kozakov, D., du, Y., Min, J., et al. (2011). Blocking eIF4E-eIF4G interaction as a strategy to impair coronavirus replication. *J. Virol.* 85, 6381–6389. doi: 10.1128/JVI.00078-11

Chemaitelly, H., Tang, P., Hasan, M., AlMukdad, S., Yassine, H. M., Benslimane, F. M., et al. (2021). Waning of BNT162b2 vaccine protection against SARS-CoV-2 infection in Qatar. *N. Engl. J. Med.* 385:e83. doi: 10.1056/NEJMoa2114114

Ciccosanti, F., di Rienzo, M., Romagnoli, A., Colavita, F., Refolo, G., Castilletti, C., et al. (2021). Proteomic analysis identifies the RNA helicase DDX3X as a host target against SARS-CoV-2 infection. *Antivir. Res.* 190, 105064–105011. doi: 10.1016/j. antiviral.2021.105064

Coronaviridae Study Group of the International Committee on Taxonomy of Viruses (2020). The species severe acute respiratory syndrome-related coronavirus: classifying 2019-nCoV and naming it SARS-CoV-2. *Nat. Microbiol.* 5, 536–544. doi: 10.1038/s41564-020-0695-z

Fabregat, A., Sidiropoulos, K., Viteri, G., Forner, O., Marin-Garcia, P., Arnau, V., et al. (2017). Reactome pathway analysis: a high-performance in-memory approach. *BMC Bioinformatics* 18, 142. doi: 10.1186/s12859-017-1559-2

Fowlkes, F., Gaglani, M., Groover, K., Thiese, M. S., Tyner, H., Ellingson, K., et al. (2021). Effectiveness of COVID-19 vaccines in preventing SARS-CoV-2 infection among frontline workers before and during B.1.617.2 (Delta) variant predominance - eight U.S. locations, December 2020-august 1021. *MMWR Morb. Mortal. Wkly Rep.* 70, 1167–1169. doi: 10.15585/mmwr.mm7034e4

Garibaldi, B. T., Wang, K., Robinson, M. L., Zeger, S. L., Bandeen-Roche, K., Wang, M. C., et al. (2021). Comparison of time to clinical improvement With vs Without Remdesivir treatment in hospitalized patients With COVID-19. *JAMA Netw. Open* 4:e213071. doi: 10.1001/jamanetworkopen.2021.3071

Geissler, R., Golbik, R. P., and Behrens, S. E. (2012). The DEAD-box helicase DDX3 supports the assembly of functional 80S ribosomes. *Nucleic Acids Res.* 40, 4998–5011. doi: 10.1093/nar/gks070

Goldberg, Y., Mandel, M., Bar-On, Y. M., Bodenheimer, O., Freedman, L., Haas, E. J., et al. (2021). Waning immunity after the BNT162b2 vaccine in Israel. *N. Engl. J. Med.* 385:e85. doi: 10.1056/NEJMoa2114228

Gordon, D. E., Hiatt, J., Bouhaddou, M., Rezelj, V. V., Ulferts, S., Braberg, H., et al. (2020a). Comparative host-coronavirus protein interaction networks reveal pan-viral disease mechanisms. *Science* 370:9403. doi: 10.1126/science.abe9403

Gordon, D. E., Jang, G.M., Bouhaddou, M., Xu, J., Obernier, K., O'Meara, M.J., et al. (2020b). A SARS-CoV-2-human protein-protein interaction map reveals drug targets and potential drug-repurposing. *bioRxiv*, doi: 10.1101/2020.03.22.002386 [Epub ahead of print].

Heerma van Voss, M. R., Vesuna, F., Bol, G. M., Afzal, J., Tantravedi, S., Bergman, Y., et al. (2018). Targeting mitochondrial translation by inhibiting DDX3: a novel radiosensitization strategy for cancer treatment. *Oncogene* 37, 63–74. doi: 10.1038/onc.2017.308

Herdy, B., Mayer, C., Varshney, D., Marsico, G., Murat, P., Taylor, C., et al. (2018). Analysis of NRAS RNA G-quadruplex binding proteins reveals DDX3X as a novel interactor of cellular G-quadruplex containing transcripts. *Nucleic Acids Res.* 46, 11592–11604. doi: 10.1093/nar/gky861

Hoffmann, M., Kleine-Weber, H., Schroeder, S., Krüger, N., Herrler, T., Erichsen, S., et al. (2020). SARS-CoV-2 cell entry depends on ACE2 and TMPRSS2 and is blocked by a clinically proven protease inhibitor. *Cell* 181:e278, 271–280.e8. doi: 10.1016/j.cell.2020.02.052

Huang, C., Lokugamage, K. G., Rozovics, J. M., Narayanan, K., Semler, B. L., and Makino, S. (2011). SARS coronavirus nsp1 protein induces template-dependent endonucleolytic cleavage of mRNAs: viral mRNAs are resistant to nsp1-induced RNA cleavage. *PLoS Pathog.* 7:e1002433. doi: 10.1371/journal.ppat.1002433

Humphrey, W., Dalke, A., and Schulten, K. (1996). VMD: visual molecular dynamics. *J. Mol. Graph.* 14, 33–38. doi: 10.1016/0263-7855(96)00018-5

Jassal, B., Matthews, L., Viteri, G., Gong, C., Lorente, P., Fabregat, A., et al. (2020). The reactome pathway knowledgebase. *Nucleic Acids Res.* 48, D498–D503. doi: 10.1093/nar/gkz1031

Ji, D., Juhas, M., Tsang, C. M., Kwok, C. K., Li, Y., and Zhang, Y. (2021). Discovery of G-quadruplex-forming sequences in SARS-CoV-2. *Brief. Bioinform.* 22, 1150–1160. doi: 10.1093/bib/bbaa114

Joshi, N., Tyagi, A., and Nigam, S. (2021). Molecular level dissection of critical spike mutations in SARS-CoV-2 variants of concern (VOCs): A simplified review. *Chem. Select* 6, 7981–7998. doi: 10.1002/slct.202102074

Juarez, D., Long, K. C., Aguilar, P., Kochel, T. J., and Halsey, E. S. (2013). Assessment of plaque assay methods for alphaviruses. *J. Virol. Methods* 187, 185–189. doi: 10.1016/j.jviromet.2012.09.026

Kamel, W., Noerenberg, M., Cerikan, B., Chen, H., Järvelin, A. I., Kammoun, M., et al. (2021). Global analysis of protein-RNA interactions in SARS-CoV-2-infected cells reveals key regulators of infection. *Mol. Cell* 81:e2857, 2851–2867.e7. doi: 10.1016/j.molcel.2021.05.023

Kondaskar, A., Kondaskar, S., Kumar, R., Fishbein, J. C., Muvarak, N., Lapidus, R. G., et al. (2010). Novel, broad Spectrum anti-cancer agents containing the tricyclic 5:7:5-fused Diimidazodiazepine ring system. *ACS Med. Chem. Lett.* 2, 252–256. doi: 10.1021/ml100281b

Kukhanova, M. K., Karpenko, I. L., and Ivanov, A. V. (2020). DEAD-box RNA helicase DDX3: functional properties and development of DDX3 inhibitors as antiviral and anticancer drugs. *Molecules* 25:1015. doi: 10.3390/molecules25041015

Kumar, N., Sharma, S., Kumar, R., Tripathi, B. N., Barua, S., Ly, H., et al. (2020). Host-directed antiviral therapy. *Clin. Microbiol. Rev.* 33:19. doi: 10.1128/CMR.00168-19

Lai, M. C., Chang, W. C., Shieh, S. Y., and Tarn, W. Y. (2010). DDX3 regulates cell growth through translational control of cyclin E1. *Mol. Cell. Biol.* 30, 5444–5453. doi: 10.1128/MCB.00560-10

Lai, M. C., Lee, Y. H., and Tarn, W. Y. (2008). The DEAD-box RNA helicase DDX3 associates with export messenger ribonucleoproteins as well as tip-associated protein and participates in translational control. *Mol. Biol. Cell* 19, 3847–3858. doi: 10.1091/mbc.E07-12-1264

Lee, C. S., Dias, A. P., Jedrychowski, M., Patel, A. H., Hsu, J. L., and Reed, R. (2008). Human DDX3 functions in translation and interacts with the translation initiation factor eIF3. *Nucleic Acids Res.* 36, 4708–4718. doi: 10.1093/nar/gkn454

Liu, G., du, W., Sang, X., Tong, Q., Wang, Y., Chen, G., et al. (2022). RNA G-quadruplex in TMPRSS2 reduces SARS-CoV-2 infection. *Nat. Commun.* 13, 1444. doi: 10.1038/s41467-022-29135-5

Mahase, E. (2021). Covid-19: Molnupiravir reduces risk of hospital admission or death by 50% in patients at risk, MSD reports. *BMJ* 375:n2422. doi: 10.1136/bmj.n2422

Malin, J. J., Suarez, I., Priesner, V., Fatkenheuer, G., and Rybniker, J. (2020). Remdesivir against COVID-19 and other viral diseases. *Clin. Microbiol. Rev.* 34:20. doi: 10.1128/CMR.00162-20

Mendoza, E. J., Manguiat, K., Wood, H., and Drebot, M. (2020). Two detailed plaque protocols for the quantification of infectious SARS-CoV-2. *Curr. Protoc. Microbiol.* 57:ecpmc105. doi: 10.1002/cpmc.105

Petrosillo, N., Viceconte, G., Ergonul, O., Ippolito, G., and Petersen, E. (2020). COVID-19, SARS and MERS: are they closely related? *Clin. Microbiol. Infect.* 26, 729–734. doi: 10.1016/j.cmi.2020.03.026

Qiao, Y., Wang, X. M., Mannan, R., Pitchiaya, S., Zhang, Y., Wotring, J. W., et al. (2020). Targeting transcriptional regulation of SARS-CoV-2 entry factors ACE2 and TMPRSS2. *Proc. Natl. Acad. Sci. U. S. A.* 118:118. doi: 10.1073/pnas.2021450118

Quaranta, P., Lottini, G., Chesi, G., Contrafatto, F., Russotto, R., Macera, L., et al. (2020). DDX3 inhibitors show antiviral activity against positive-sense single-stranded RNA viruses but not against negative-sense single-stranded RNA viruses: The coxsackie B model. *Antivir. Res.* 178:104750. doi: 10.1016/j.antiviral.2020.104750

Russon, M. P., Westerhouse, K. M., and Tran, E. J. (2021). Transcription, translation, and DNA repair: new insights from emerging noncanonical substrates of RNA helicases. *Biol. Chem.* 402, 637–644. doi: 10.1515/hsz-2020-0333

Schmidt, N., Lareau, C. A., Keshishian, H., Ganskih, S., Schneider, C., Hennig, T., et al. (2021). The SARS-CoV-2 RNA-protein interactome in infected human cells. *Nat. Microbiol.* 6, 339–353. doi: 10.1038/s41564-020-00846-z

Schroder, M. (2011). Viruses and the human DEAD-box helicase DDX3: inhibition or exploitation? *Biochem. Soc. Trans.* 39, 679–683. doi: 10.1042/BST0390679

Shen, L. W., Qian, M. Q., Yu, K., Narva, S., Yu, F., Wu, Y. L., et al. (2020). Inhibition of influenza A virus propagation by benzoselenoxanthenes stabilizing TMPRSS2 gene G-quadruplex and hence down-regulating TMPRSS2 expression. *Sci. Rep.* 10, 7635. doi: 10.1038/s41598-020-64368-8

Shih, J. W., Wang, W. T., Tsai, T. Y., Kuo, C. Y., Li, H. K., and Wu Lee, Y. H. (2012). Critical roles of RNA helicase DDX3 and its interactions with eIF4E/PABP1 in stress granule assembly and stress response. *Biochem. J.* 441, 119–129. doi: 10.1042/BJ20110739

Singh, Y., Fuloria, N. K., Fuloria, S., Subramaniyan, V., Meenakshi, D. U., Chakravarthi, S., et al. (2021). N-terminal domain of SARS CoV-2 spike protein mutation associated reduction in effectivity of neutralizing antibody with vaccinated individuals. *J. Med. Virol.* 93, 5726–5728. doi: 10.1002/jmv.27181

Soto-Rifo, R., and Ohlmann, T. (2013). The role of the DEAD-box RNA helicase DDX3 in mRNA metabolism. *Wiley Interdiscip. Rev. RNA* 4, 369–385. doi: 10.1002/wrna.1165

Soto-Rifo, R., Rubilar, P. S., Limousin, T., de Breyne, S., Décimo, D., and Ohlmann, T. (2012). DEAD-box protein DDX3 associates with eIF4F to promote translation of selected mRNAs. *EMBO J.* 31, 3745–3756. doi: 10.1038/emboj.2012.220

Spinner, C. D., Gottlieb, R. L., Criner, G. J., Arribas López, J. R., Cattelan, A. M., Soriano Viladomiu, A., et al. (2020). Effect of Remdesivir vs standard care on clinical status at 11 days in patients With moderate COVID-19: A randomized clinical trial. *JAMA* 324, 1048–1057. doi: 10.1001/jama.2020.16349

Squeglia, F., Romano, M., Ruggiero, A., Maga, G., and Berisio, R. (2020). Host DDX helicases as possible SARS-CoV-2 Proviral factors: A structural overview of their hijacking Through multiple viral proteins. *Front. Chem.* 8:602162. doi: 10.3389/fchem.2020.602162

Stammler, S. N., Cao, S., Chen, S. J., and Giedroc, D. P. (2011). A conserved RNA pseudoknot in a putative molecular switch domain of the 3′-untranslated region of coronaviruses is only marginally stable. *RNA* 17, 1747–1759. doi: 10.1261/rna.2816711

Szklarczyk, D., Gable, A. L., Lyon, D., Junge, A., Wyder, S., Huerta-Cepas, J., et al. (2019). STRING v11: protein-protein association networks with increased coverage, supporting functional discovery in genome-wide experimental datasets. *Nucleic Acids Res.* 47, D607–D613. doi: 10.1093/nar/gky1131

Valiente-Echeverria, F., Hermoso, M. A., and Soto-Rifo, R. (2015). RNA helicase DDX3: at the crossroad of viral replication and antiviral immunity. *Rev. Med. Virol.* 25, 286–299. doi: 10.1002/rmv.1845

van den Born, E., Posthuma, C. C., Gultyaev, A. P., and Snijder, E. J. (2005). Discontinuous subgenomic RNA synthesis in arteriviruses is guided by an RNA hairpin structure located in the genomic leader region. *J. Virol.* 79, 6312–6324. doi: 10.1128/JVI.79.10.6312-6324.2005

Wang, Y., Zhang, D., du, G., du, R., Zhao, J., Jin, Y., et al. (2020). Remdesivir in adults with severe COVID-19: a randomised, double-blind, placebo-controlled, multicentre trial. *Lancet* 395, 1569–1578. doi: 10.1016/S0140-6736(20)31022-9

Whelan, S., and Goldman, N. (2001). A general empirical model of protein evolution derived from multiple protein families using a maximum-likelihood approach. *Mol. Biol. Evol.* 18, 691–699. doi: 10.1093/oxfordjournals.molbev.a003851

Winnard, P. T. Jr., Vesuna, F., and Raman, V. (2021). Targeting host DEAD-box RNA helicase DDX3X for treating viral infections. *Antivir. Res.* 185:104994. doi: 10.1016/j.antiviral.2020.104994

Xie, M., Vesuna, F., Tantravedi, S., Bol, G. M., Heerma van Voss, M. R., Nugent, K., et al. (2016). RK-33 Radiosensitizes prostate cancer cells by blocking the RNA helicase DDX3. *Cancer Res.* 76, 6340–6350. doi: 10.1158/0008-5472.CAN-16-0440

Yang, S. N. Y., Atkinson, S. C., Audsley, M. D., Heaton, S. M., Jans, D. A., and Borg, N. A. (2020). RK-33 is a broad-Spectrum antiviral agent That targets DEAD-box RNA helicase DDX3X. *Cell* 9:10170. doi: 10.3390/cells9010170

Yang, D., and Leibowitz, J. L. (2015). The structure and functions of coronavirus genomic 3′ and 5′ ends. *Virus Res.* 206, 120–133. doi: 10.1016/j.virusres.2015.02.025

Yoshimoto, F. K. (2020). The proteins of severe acute respiratory syndrome Coronavirus-2 (SARS CoV-2 or n-COV19), the cause of COVID-19. *Protein J.* 39, 198–216. doi: 10.1007/s10930-020-09901-4

Zheng, W., Zhang, C., Li, Y., Pearce, R., Bell, E. W., and Zhang, Y. (2021). Folding non-homologous proteins by coupling deep-learning contact maps with I-TASSER assembly simulations. *Cell Rep. Methods.* 1, 100014. doi: 10.1016/j.crmeth.2021.100014